IEEE Access
Multidisciplinary | Rapid Review | Open Access Journal

Received January 4, 2020, accepted January 13, 2020, date of publication January 17, 2020, date of current version January 27, 2020.

Digital Object Identifier 10.1109/ACCESS.2020.2967410

Unmanned Aerial Vehicle (UAV) Photogrammetry Technology for Dynamic Mining Subsidence Monitoring and Parameter Inversion: A Case Study in China

ZHOU DAWEI[1], QI LIZHUANG[1], ZHANG DEMIN[2], ZHOU BAOHUI[2], AND GUO LIANGLIN[1]

[1]Jiangsu Key Laboratory of Resources and Environmental Information Engineering, China University of Mining and Technology, Xuzhou 221116, China
[2]Xinneng Mining Industry Corporation Limited, Ordos City 017000, China

Corresponding authors: Zhou Dawei (dwzhou2008@cumt.edu.cn) and Qi Lizhuang (1963524159@qq.com)

This work was supported in part by the Natural Science Foundation of China under Grant 51604266, in part by the Open Fund of Jiangsu Key Laboratory of Resources and Environmental Information Engineering under Grant JS201709, in part by the Fundamental Research Funds for The Central Universities under Grant 2017QNA34, and in part by the Natural Science Foundation of Jiangsu Province under Grant BK20190642.

ABSTRACT This study mainly presents the method for monitoring the surface dynamic subsidence basin (SDSB) caused by underground coal mining and obtaining parameters of mining subsidence (PMS) in the short term by using an unmanned aerial vehicle (UAV) Photogrammetry Technology. The basic ideas and methods are proposed; that is, the two-stage surface digital elevation model (DEM) is obtained in the short term by UAV; The SDSB is obtained through two phases of DEM subtraction; Based on the dynamic inversion method established in this study, the PMS was obtained. The UAV method was used to monitor the Wangjiata coal mine in Inner Mongolia of China three times in three months to obtain the three phases of DEM; we obtained the two phases SDSB by the three phases of DEM subtraction. The accuracy of DEM and SDSB were 118 mm and 121 mm respectively, Although the accuracy cannot fulfill the requirements of mining subsidence, the PMS was obtained by dynamic inversion method of full subsidence basin fitting, which has better resistance to errors; hence, the obtained PMS are reliable. Based on the engineering application, this study concludes that as a new technology, UAV photogrammetry technology can obtain the SDSB of coal mining areas in a short period with reliable PMS. Meanwhile, it has the advantages of low cost, flexible maneuverability, and so on, and overcomes the shortages of traditional observation stations, which has long observation time and high labor intensity, needs to bury fixed measuring points and easily lose them, and just has a small amount of ''spot-like'' observation data that cannot reflect the deformation characteristics of the whole subsidence basin. Furthermore, it is feasible to apply this method to mining subsidence monitoring and parameter inversion, and it has a great application prospect for the mining area purposes.

INDEX TERMS UAV photogrammetry technology, surface dynamic subsidence basin, parameters of mining subsidence, probability integration model, dynamic inversion method.

I. INTRODUCTION

The coal mining–induced surface subsidence is a complex spatiotemporal process and causes ecological environment damage. To study the complex process and assess the damage degree of the surface subsidence, it is essential to obtain the surface subsidence value and the surface subsidence parameters. In addition, predicting mining subsidence is one of the core contents of mining subsidence, which is of considerable significance to the theoretical study and production of mining subsidence, and can be used to ascertain whether ground structures are affected by mining and determine the corresponding extent [1], [2]. In addition, predicting mining subsidence is the basis for repairing, reinforcing, rebuilding

The associate editor coordinating the review of this manuscript and approving it for publication was Zhen Li.

on-site, or taking underground measures. The PMS is crucial to determine the accuracy of the prediction.

The determining method of prediction parameters on mining subsidence is to establish observation stations for surface subsidence to obtain the surface movement data, followed by calculating the PMS based on the measured data [1], [3]. The process for determining prediction parameters of mining subsidence include the following: (1) establishment of parameters acquisition model, and (2) measured data acquisition.

Currently, the probabilistic integral steady-state model is the leading method to obtain prediction parameters [1], [3]–[5]; that is, the model parameters are evaluated using the final subsidence data after the mining-caused surface movement deformation. Thus, the method needs to acquire the surface-stable subsidence data for parameter calculation. Nevertheless, based on the measured data and the studies of domestic experts, it can be asserted that the surface subsidence stabilization time caused by mining in China's major mining areas is usually $\geq$2 years [1], [3], [6]; this method requires, at least, 2 years of surface movement observation to attain a set of surface subsidence parameters.

Currently, the observation stations primarily adopt traditional observation stations, and the leading layout is the section linear observation stations comprising two mutually perpendicular observation lines on the main section of the mining working face [1]–[3], [7]–[9]. The observation methods include leveling measurement and traverse measurement (or the total station traverse measurement). The observed data only includes the distribution and size of the movement and deformation on the section where the observation line is located. Of note, traditional observatories have several disadvantages. The observation period is long ($\geq$2 years), and the field observation labor intensity is large. Meanwhile, it is essential to bury a fixed measuring point, which would occupy land and be easily lost. Of note, elevation measurements and plane measurements are often performed separately so that the results do not entirely reflect the spatiotemporal relationship of the measuring points. Moreover, the observed data are only the information on the main section and are dot data, which do not entirely reflect the limitations of the entire basin. The traditional method to attain a set of mining subsidence parameters has the disadvantages of time and energy consumption and small amount of data. Thus, new surveying and mapping technologies and methods are warranted in monitoring the mining subsidence to overcome the limitations of traditional observation stations mentioned above.

With the rapid advancements of science and technology in recent years, several new measuring techniques have been applied in deformation monitoring, which can be summarized as follows. (1) Compared with traditional measurement methods, 3D laser scanning technology [8], [10] offers unique advantages such as it does not need to bury fixed measuring points, can execute planar scanning, and obtain deformation information in a large range with large data volume and high precision. However, when using 3D laser scanning for data acquisition, owing to the limited viewing angle or other object occlusions, it is essential to properly arrange the site for full-scale scanning. Thus, there are two common approaches to solve the problem of inconsistent cloud coordinates for each site: (i) set up multiple public targets between stations, and (ii) establish a control network first. However, some problems exist in both methods as follows: (i) the field labor is large; (ii) the observation efficiency is low, making it unable to be used in a large area; and (iii) it is difficult to layout the target uniformly and measure the center coordinate of the target in mountainous areas with complex topography. Consequently, these limitations restrict the promotion and application of 3D laser scanning technology in mining areas. (2) InSAR technology (synthetic aperture radar interference)[10]–[20] can offer all-weather and all-day imaging with large imaging areas, abundant information, and high precision. Nevertheless, the large subsidence of mining subsidence in the mining area accounts for phase unwrapping errors. Hence, the monitoring results have a large deviation, and even the large deformation of the mining area cannot be monitored, which has become one of leading factors limiting the application of InSAR technology in mining subsidence monitoring.

Contrary to 3D laser scanning technology and InSAR technology, unmanned aerial vehicle Photogrammetry technology (UAV) [21]–[24] offers multiple advantages such as low cost, flexibility, and quickly obtaining a wide range of high-quality surface subsidence information. UAV Photogrammetry technology was adopted for mining subsidence observation, which does not need fixed measuring points or observation of the entire process from the beginning of mining to the end of mining stability. In a short period (months), some subsidence areas are selected to monitor two to three times, and after data processing, digital elevation model (DEM) is used to assess each mining area. However, some subsidence areas are selected and monitored for two or three periods within a short time (several months), and DEM of each period is attained through data processing. Then, the dynamic subsidence data of mining area can be obtained by DEM subtraction of two periods. The subsidence parameters of surface mining can be obtained by establishing the basin dynamic parameters of the probability integral model. UAV Photogrammetry technology can not only enhance the efficiency but also obtain rich observation data of subsidence basin, which is equivalent to a high-density planar observation station. Besides, this method provides more comprehensive measured data and precise predicted parameters for mining subsidence. Thus, UAV Photogrammetry technology offers a broader application prospect in the mining area because it can better predict surface subsidence. In this study, taking Wangjiata Coal Mine as an example, we examined the method of applying UAV Photogrammetry Technology to monitor mining subsidence and surface mining subsidence parameters inversion in the mining area.

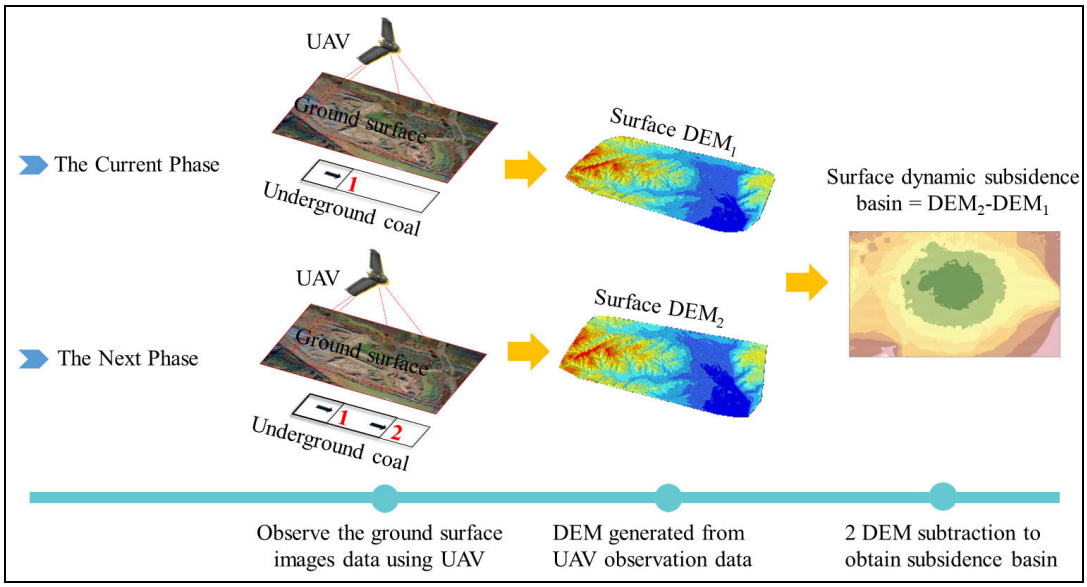

FIGURE 1. Sketch of UAV Photogrammetry technology for monitoring SDSB.

II. BASIC IDEAS AND METHODS OF SDSB AND PMS

Figure 1 shows the schematic diagram of monitoring surface subsidence caused by coal mining using UAV Photogrammetry technology. When coal seam is excavated toward position 1, observe the ground surface above the coal seam using UAV, and then establish digital elevation model (DEM) in the mining subsidence area by observed data (hereinafter DEM1). While the coal seam is pushed to position 2, the new DEM (hereinafter DEM2) is obtained by the second observation of the ground surface at the same surface position. By deducting DEM2 from DEM1, we measured SDSB during a period between two mining processes (positions 1 and 2). Combined with underground mining and dynamic inversion method, PMS can be deduced.

III. DYNAMIC INVERSION METHOD OF PMS

A. DYNAMIC PREDICTION METHOD

The dynamic prediction method (referred to as DPM) of probability integral considers the correlation between the process of surface subsidence and the spatial position, as well as time. The DPM is the final state of surface subsidence caused by underground coal mining, namely probability integral steady-state prediction model (PIM), multiplied by the time effect function.

1) PIM

The PIM is named for the probability integral in its prediction formula, which is based on the random medium theory [1]–[3], [5], [7]]; this model has been extensively used in China. The PIM can be used to illustrate the prediction model of an arbitrary point on the surface, and the formula of unit mining surface subsidence basin can be obtained as follows:

$$W_e(x) = \frac{1}{r} e^{\pi \frac{x^2}{r^2}} \tag{1}$$

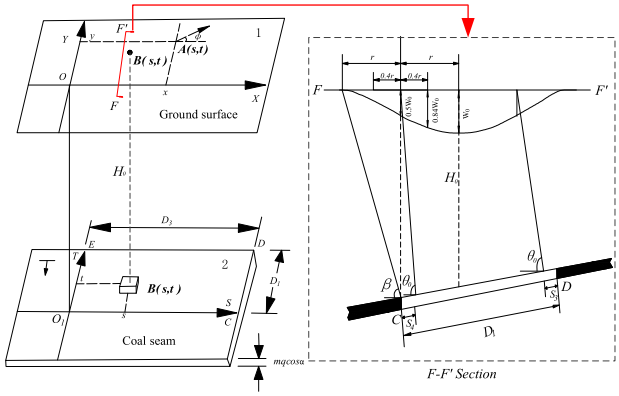

FIGURE 2. Spatial coordinates (1 is the surface, and 2 is the underground coal seam) [7].

Considering the 3D characteristics in Figure 2, the surface subsidence of any point $A(x, y)$ because of the unit mining $B(s, t)$ can be expressed as follows:

$$W_e(x, y) = \frac{1}{r^2} e^{\pi \frac{(x-S)^2+(y-t)^2}{r^2}} \tag{2}$$

When the mining is O1CDE, the subsidence prediction formula of point A caused by the whole mining is as follows:

$$W(x, y) = W_0 \int_0^l \int_0^L \frac{1}{r^2} e^{\pi \frac{(x-S)^2+(y-t)^2}{r^2}} dtds \tag{3}$$

where W_0 is the maximum subsidence at supercritical mining, $W_0 = mqcosa$; r is the main influence radius, $r = H_0/tan\beta$; l is strike length, $l = D_3 - S_3 - S_4$; L is the dip length, $L = (D_1\text{-}S_1\text{-}S_2)\cdot sin(\theta_0 + a)/sin(\theta_0)$. Based on the subsidence formula, other displacement deformation values of the surface (X, Y) can be deduced.

To use this model to obtain the full subsidence, it is essential to confirm the prediction parameters q, $tan\beta$, $S1$, $S2$, $S3$, $S4$, and θ_0. Here, q is the subsidence coefficient; $tan\beta$ is the tangent of the main influence angle; θ_0 is the mining transference angle; and (S1, S2, S3, S4) is the deviation of the inflection point.

2) TIME EFFECT FUNCTION

The surface subsidence is a continuous spatiotemporal process, which depends on the spatial location and time, as well as on the mining speed and overburden property. Movement and deformation are continuous spatiotemporal functions. The dynamic prediction model is to establish the correlation between subsidence and spatial position and time.

If a minuscule working face of the coal seam (or dividing the working face into n minuscule working faces) is produced instantaneously, $We(x, y)$ and $Weo(x, y, t)$ are the final subsidence value of the surface point $p(x,y)$ caused by the mining working face and the subsidence value at time t, respectively. The time effect function is$f(t)$, then

$$Weo(x, y, t) = We(x, y) \bullet f(t) \tag{4}$$

Of note, $We(x, y)$ is the steady-state prediction model of probabilistic integral, and the time effect function is $f(t) = 1 - e^{-ct}$, where t is the time interval between the estimated time and the unit mining time; and C is the subsidence velocity coefficient.

If one working face is divided into n small rectangular faces and mining is just located in rectangular working face i at time t, then, the subsidence value of point$p$ on the surface at time $t$caused by the mining areas ($1 \sim i$ small rectangular working face) can be evaluated according to the superposition principle.

$$W(x, y, t) = \sum_{i=1}^{n} (Wie(x, y) \bullet f(t_i)) \tag{5}$$

The subsidence value of any point on the surface at any time can be obtained by finding the subsidence velocity coefficient C, while C is the time effect coefficient depending on the rock properties, which is calculated as follows.

The following formula is to evaluate the subsidence velocity coefficient [3], [10]:

$$C = 2.0 \bullet v \bullet \tan\beta / H \tag{6}$$

where, v is the average advance speed of the working face (m/d); $tan\beta$ is the tangent of the main influence angle; and H is the average mining depth.

B. INVERSION METHOD BASED ON DPM

Set n observation points on the ground movement observation station above coal mining working face, and the field measured subsidence of an arbitrarily observation point i (i = 1, 2, 3, ..., n) is marked as $W_{i-measured}$; based on the probability integral method [namely Eq. (5)], the predicted subsidence marked as $W_{i-predicted}$ of the arbitrarily point i can be expressed as a function of the independent variable X (x, y) (coordinates of observation points) and the subsidence prediction parameters (q, β, S_1, S_2, S_3, S_4,θ_0), so Eq. (5) can be abbreviated to:

$$W_{i-predicted} = f(X_i, q, \tan\beta, S_1, S_2, S_3, S_4, \theta_0) \tag{7}$$

To build an inversion calculation model of subsidence parameters, we expanded Eq. (7) into the Taylor's Series, take the first derivative item, and substitute the initial subsidence parameters and coordinates of observation points into the equation, Eq. (7) can be rewritten as follows:

$$\begin{aligned} &W_{i-predicted} \\ &= f[X_i, (q)_0, (\tan\beta)_0, (S_1)_0, (S_2)_0, (S_3)_0, (S_4)_0, (\theta_0)_0] \\ &+ \frac{\partial f}{\partial q}\Delta q + \frac{\partial f}{\partial \tan\beta}\Delta\tan\beta + \frac{\partial f}{\partial S_1}\Delta S_1 \\ &+ \frac{\partial f}{\partial S_2}\Delta S_2 + \frac{\partial f}{\partial S_3}\Delta S_3 + \frac{\partial f}{\partial S_4}\Delta S_4 + \frac{\partial f}{\partial \theta_0}\Delta\theta_0 \end{aligned} \tag{8}$$

where $(q)_0, (\tan\beta)_0, (S_1)_0, (S_2)_0, (S_3)_0, (S_4)_0, (\theta_0)_0$ are respectively the initial approximation subsidence parameters.

Based on the measured subsidence $W_{i-measured}$ and the predicted subsidence $W_{i-redicted}$, an error equation can be obtained as follows:

$$\begin{aligned} V_i = W_{i-predicted} - W_{i-measured} &= (W_{i-predicted})_0 \\ &+ \frac{\partial f}{\partial q}\Delta q + \frac{\partial f}{\partial \tan\beta}\Delta\tan\beta + \frac{\partial f}{\partial S_1}\Delta S_1 + \frac{\partial f}{\partial S_2}\Delta S_2 \\ &+ \frac{\partial f}{\partial S_3}\Delta S_3 + \frac{\partial f}{\partial S_4}\Delta S_4 + \frac{\partial f}{\partial \theta_0}\Delta\theta_0 - W_{i-measured} \end{aligned} \tag{9}$$

where

$$\begin{aligned} &(W_{i-predicted})_0 \\ &= f[X_i, (q)_0, (\tan\beta)_0, (S_1)_0, (S_2)_0, (S_3)_0, (S_4)_0, (\theta_0)_0]. \end{aligned}$$

Assume $l_i = (W_{i-predicted})_0 - W_{i-measured}$ (i = 1,2, 3,.....,n), matrix form of Eq. (9) is as follows, (10), as shown at the bottom of the next page. Based on the principle of least squares, that is,$V^T V$ = min, we can obtain the normal equation:

$$B^T BZ + B^T L = 0 \tag{11}$$

Solving Eq. (11), we can obtain the parameters correction; adding the correction to the initial approximation parameters, we obtained the accurate parameters.

C. STEPS OF PMS ACQUISITION

The steps of the dynamic acquisition method of parameters are as follows:

(1) Based on the overall monitoring area to generate the predicted grid, it is normally essential to set a rectangular range containing the monitoring area to generate the grid.

(2) Based on the DEM obtained by two observations, the grid elevation value is obtained through interpolation.

(3) Input the working face information and dimension. Then, input the time t_1 and t_2 when the mining location starts mining of the working face.

TABLE 1. The necessary information of the working face 2S201.

Strike	Dip	Mean mining depth	Mean ground elevation	Mean Mining Thickness of Coal Seam	Mean mining speed	coal seam dip angle
1253 m	260 m	200 m	+1309 m~+1392 m	3.26 m	(12-15) m/d	2°

(4) Input the initial values and upper and lower bounds of parameters.

(5) The subsidence value W_1 and W_2 of grid points at t_1 and t_2 are predicted, respectively, and the difference between W_2 and W_1 is the subsidence in time $t_1$to t_2.

(6) The measured subsidence is obtained by subtracting two measured elevations.

(7) The difference between measured subsidence and calculated subsidence is the fitting error.

(8) Based on the fitting error, determine whether to continue the iteration. If the need is to continue iterating, reselect the parameters and star from step (5).

Figure 3 displays the flowchart of dynamic parameter acquisition.

Based on these steps, we can obtain the final parameters of surface subsidence, including subsidence coefficient q, the tangent of the main influence angle $tan\beta$, the mining transference angle θ, and the deviation of inflection point S. However, it does not include horizontal displacement coefficient.

IV. ENGINEERING APPLICATION ANALYSIS

A. GENERAL SITUATION OF THE STUDY AREA

Wangjiata coal mine is located in Ordos, Inner Mongolia autonomous province of China. The characteristics of the working face 2S201 are as follows: strike length, ~1253 m; dip length, ~260 m; and the average dip angle of the coal seam, 2°. In addition, the mining depth is approximately 200 m, and the average mining thickness is 3.26 m. Table 1 presents the detailed parameters. The mine started on July 11, 2018, and stopped October 15, 2018. Figure 4 shows the excavation view of the working face.

B. FIEDL DATA ACQUISITION USING UAV

1) FLIGHT DESIGN

In this study, UAV used was Trimble UX5 (Figure 5) to acquire photography images, and images were taken directly from SONY A5100 SLR camera. The flight scheme was designed as follows:

(1) The ground resolution was 6 cm in this flight scheme. The images were designed with an overlap of 80% and 60% in the flight and side directions, respectively.

(2) Based on the focal length (15 mm) and pixel size of the camera, the relative flight height was 230 m.

(3) Route planning and sortie division—the test course direction was designed per the wind direction, and the course direction was perpendicular to the wind direction. The area was approximately 1.66 km^2, and the flight time was 35 min.

(4) The measurement of image control points. The layout of image control points was marked on the ground by laying lime powder. Based on the area and terrain variation, eight image control points were evenly arranged in the survey area, which were measured by the total station and GPS-RTK.

2) DATA ACQUISITION

We performed a total of three phases for UAV photography to obtain 560 images in each phase (seen from Table 2);

$$\underset{n\times 1}{V} = \underset{n\times 7}{B}\,\underset{7\times 1}{Z} + \underset{n\times 1}{L}$$

$$V = \begin{pmatrix} V_1 \\ V_2 \\ \vdots \\ V_n \end{pmatrix}, \quad Z = \begin{pmatrix} \Delta q \\ \Delta \tan\beta \\ \Delta S_1 \\ \Delta S_2 \\ \Delta S_3 \\ \Delta S_4 \\ \Delta\theta_0 \end{pmatrix}, \quad L = \begin{pmatrix} l_1 \\ l_2 \\ \vdots \\ l_n \end{pmatrix}$$

$$B = \begin{pmatrix} \left(\frac{\partial f}{\partial q}\right)_1 & \left(\frac{\partial f}{\partial \tan\beta}\right)_1 & \left(\frac{\partial f}{\partial S_1}\right)_1 & \left(\frac{\partial f}{\partial S_2}\right)_1 & \left(\frac{\partial f}{\partial S_3}\right)_1 & \left(\frac{\partial f}{\partial S_4}\right)_1 & \left(\frac{\partial f}{\partial \theta_0}\right)_1 \\ \left(\frac{\partial f}{\partial q}\right)_2 & \left(\frac{\partial f}{\partial \tan\beta}\right)_2 & \left(\frac{\partial f}{\partial S_1}\right)_2 & \left(\frac{\partial f}{\partial S_2}\right)_2 & \left(\frac{\partial f}{\partial S_3}\right)_2 & \left(\frac{\partial f}{\partial S_4}\right)_2 & \left(\frac{\partial f}{\partial \theta_0}\right)_2 \\ \vdots & \vdots & \vdots & \vdots & \vdots & \vdots & \vdots \\ \left(\frac{\partial f}{\partial q}\right)_n & \left(\frac{\partial f}{\partial \tan\beta}\right)_n & \left(\frac{\partial f}{\partial S_1}\right)_n & \left(\frac{\partial f}{\partial S_2}\right)_n & \left(\frac{\partial f}{\partial S_3}\right)_n & \left(\frac{\partial f}{\partial S_4}\right)_n & \left(\frac{\partial f}{\partial \theta_0}\right)_n \end{pmatrix} \tag{10}$$

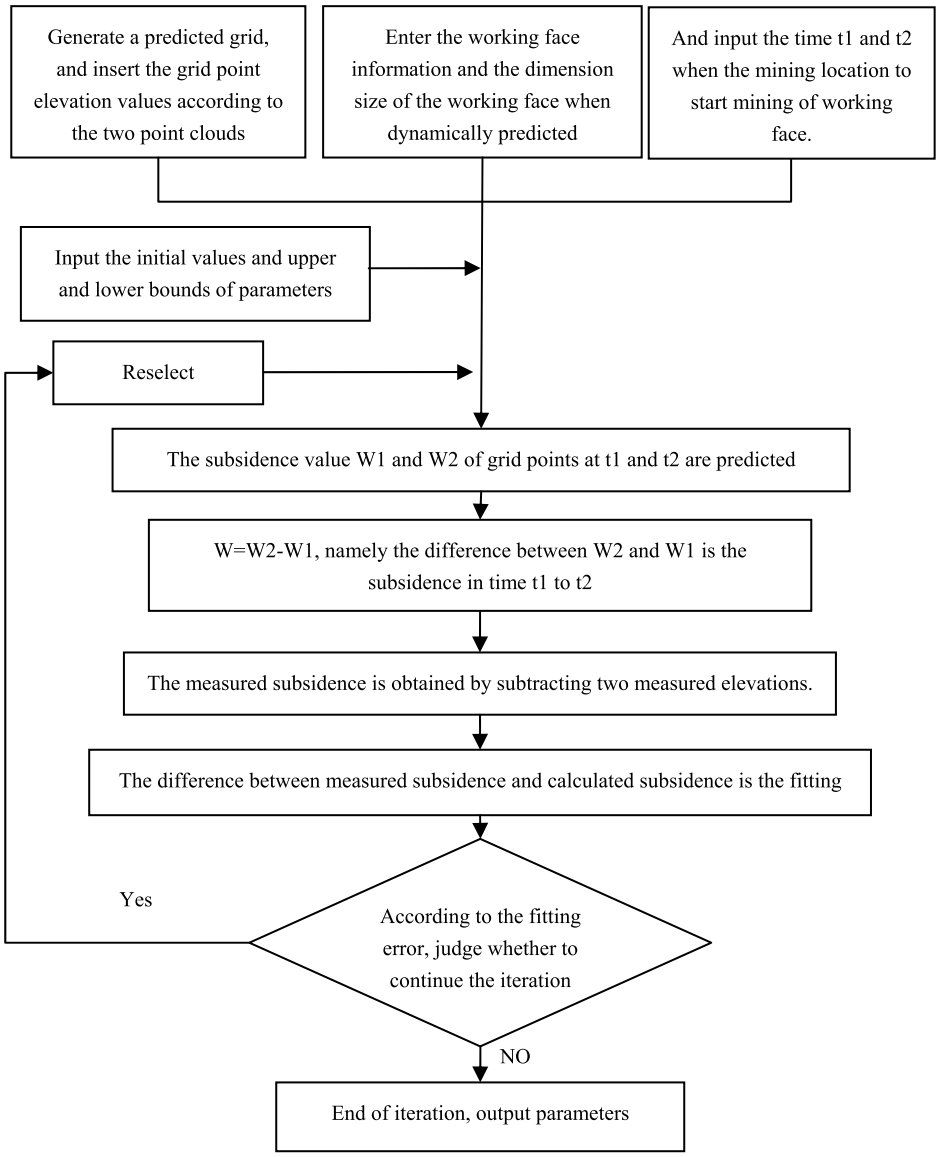

FIGURE 3. The flowchart of dynamic parameter acquisition.

The three phases of UAV photography were as follows: June 9, 2018; September 3, 2018; and October 15, 2018; Figure 4 shows the layout of flight strips of each phase, there are 28 east–west flight strips in the first and second phase, and 20 photos were taken for each flight strip. In the third phase, there are 14 north–south flight strips, each of which took 40 photos. The average flight height was nearly 230 m. In the flight area, 13 control points were set [Figure 4 and Figure 5(c)], we take total station to measure the 3D coordinate of these control points.

C. SDSB AND ITS ACCURACY ANALYSIS

1) DEM AND ITS ACCURACY ANALYSIS

The UAV photogrammetry technology needs to process a large number of images [25], [26]. However, there are already powerful and mature software for processing UAV photogrammetry image data, such as Inpho, Pix4D and PhotoScan. We generated DEM in this study using the PIX4D software. PIX4D is a professional UAV mapping and photogrammetry software, which can convert images taken by UAV, handheld device or aircraft, generate high-precision 2D maps and 3D models with geographic coordinates, and generate a broad range of customizable results, which are compatible with various software.

The three phases of UAV data were imported into the PIX4D software. The coordinate of control points was imported, the center position of the image control points was edited, and the DEM was generated through aerial triangulation (Figure 6).

Based on the high-precision testing requirements in the specifications of quality inspection and acceptance of surveying and mapping products, we evaluated the mean square

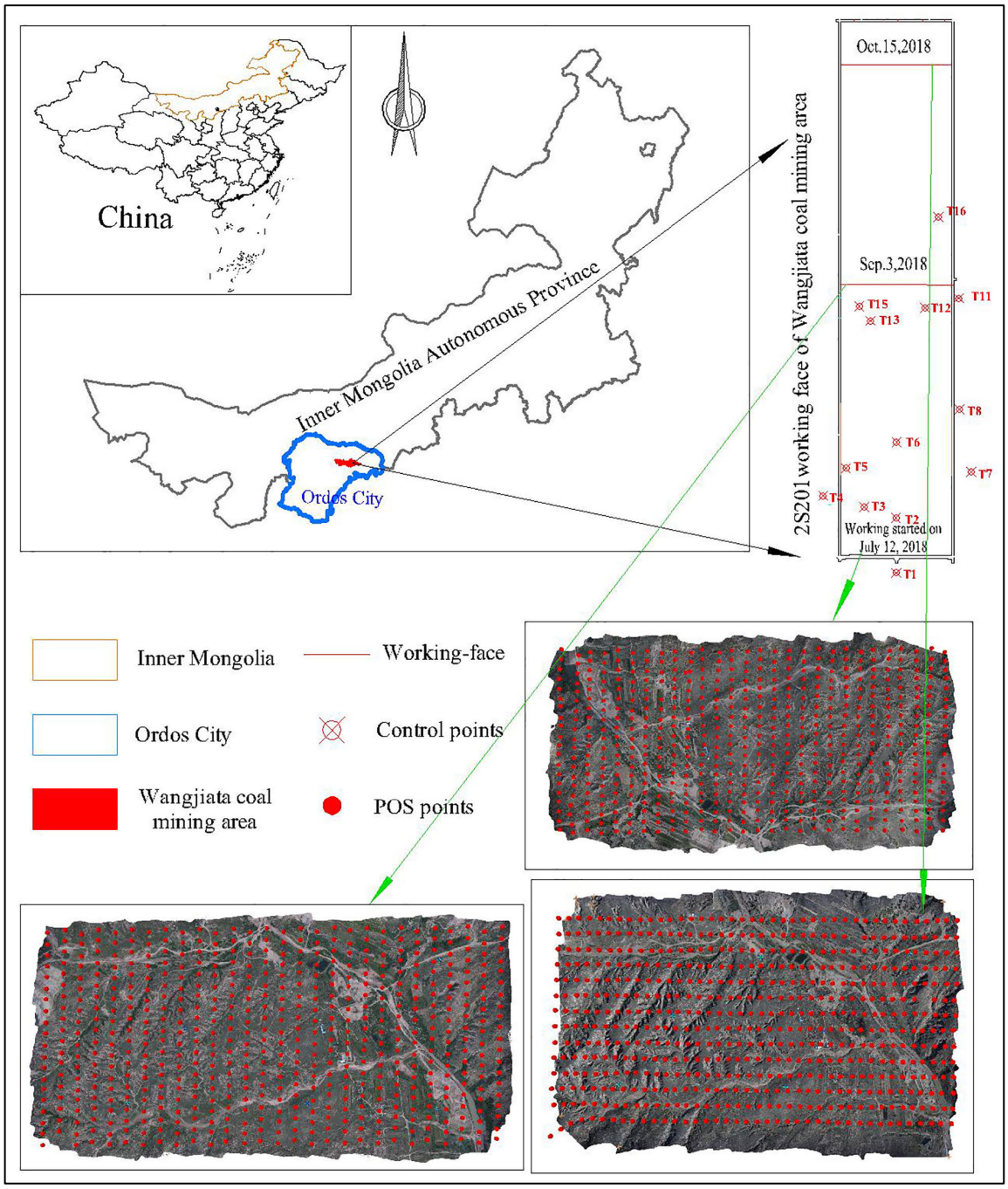

FIGURE 4. The excavation view of the working face 2S201 and layout of image control points.

TABLE 2. Data acquisition achieved over the study areas.

	Strips	Images	GCPs	Area (km^2)	Consumed Time (min)	Average Flying Height (m)
The first phase (June 9, 2018)	28	560	13	2.76	35	230
The second phase (September 3, 2018)	28	560	8	2.67	35	230
The third phase (October 15, 2018)	14	560	12	2.75	35	230

error (M) as follows:

$$M = \sqrt{\frac{\sum_{i=1}^{n} \Delta_i^2}{n}} \tag{12}$$

The DEM precision of UAV was obtained by comparing the total station data collected by the ground point and the corresponding elevation of the DEM generated by the UAV.

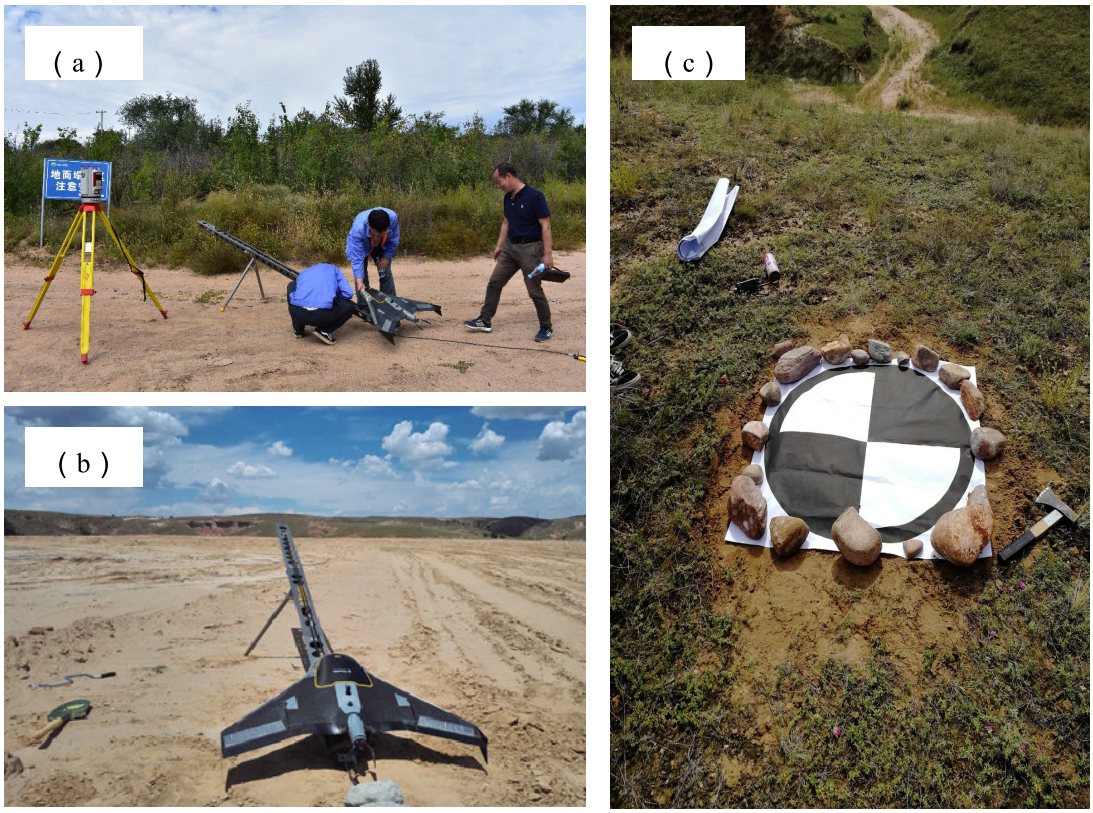

FIGURE 5. UAV photogrammetry flight scene, (a) the flight scene, (b) the UAV of Trimble UX5, and (c) markers of control points.

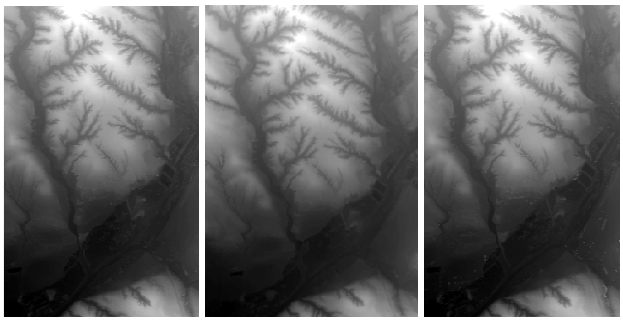

(a) The first phase (b) The second phase (c) The third phase

FIGURE 6. The DEM generated by UAV image processing.

Using formula (12), the mean square error in DEM of UAV was evaluated as follows (Tables 3−5).

Compared with the data of the total station in each period, on June 9, 2018, the DEM data of UAV in the first phase displayed the lowest precision, with an elevation mean square error of 148 mm. Conversely, the data in the third phase had the highest precision, with an elevation mean square error of 96 mm. Furthermore, the DEM average elevation mean square error of UAV data was 118 mm.

TABLE 3. DEM accuracy in the first phase on June 9, 2018.

Numbers	Elevation of total station /m	DEM elevation of UAV /m	Elevation difference /m
1	1306.717	1306.503	-0.213
2	1308.405	1308.408	0.004
3	1317.198	1317.162	-0.036
4	1313.637	1313.471	-0.166
5	1314.187	1314.031	-0.156
6	1314.218	1314.052	-0.165
7	1319.064	1318.874	-0.189
8	1330.697	1330.582	-0.114
Mean square error of height: 0.148m			

2) DYNAMIC SUBSIDENCE BASIN AND ITS ACCURACY ANALYSIS

a: SUBSIDENCE BASIN ACQUISITION

We subtracted DEM observed in phases 2 and 3 from DEM observed in phase 1 to obtain the surface subsidence basin caused by mining in the working face 2S201 (Figure 7). During June 9 to September 3, 2018, when the coal seam was excavated to 640 m, it reached supercritical mining, and the maximum subsidence value was 2135 mm. By October 15, 2018, coal seam was excavated to 780 m, and the corresponding maximum subsidence value was 2670 mm, suggesting that the maximum subsidence value was basically stable.

TABLE 4. DEM accuracy in the second phase of September 3, 2018.

Numbers	Elevation of total station /m	DEM elevation of UAV /m	Elevation difference /m
1	1306.579	1306.445	-0.133
2	1306.014	1305.905	-0.108
3	1315.281	1315.296	0.015
4	1313.413	1313.337	-0.075
5	1316.817	1316.672	-0.144
6	1311.772	1311.744	-0.027
7	1314.052	1314.045	-0.006
8	1318.94	1318.9	-0.039
9	1319.806	1319.692	-0.113
10	1330.62	1330.452	-0.167
11	1345.375	1345.205	-0.169
12	1351.667	1351.542	-0.124
Mean square error of height: 0.109m			

TABLE 5. DEM accuracy in the third phase on October 15, 2018.

Numbers	Elevation of total station /m	DEM elevation of UAV /m	Elevation difference /m
1	1306.586	1306.439	-0.146
2	1306.014	1305.843	-0.17
3	1315.23	1315.225	-0.004
5	1316.813	1316.743	-0.069
6	1311.764	1311.734	-0.029
7	1314.117	1314.123	0.006
8	1319.004	1319.012	0.008
9	1319.877	1319.767	-0.109
10	1330.61	1330.535	-0.074
11	1345.313	1345.234	-0.078
12	1343.723	1343.577	-0.145
Mean square error of height: 0.096m			

b: ACCURACY ANALYSIS OF SUBSIDENCE BASIN

The mean square errors in the data of subsidence basin using UAV can be calculated by subtracting the elevation of the total station at corresponding points in the two periods from that of corresponding DEM of UAV (refer Table 6 for more details). According to the calculation results, the maximum mean square error of the subsidence value was 0.140 m, the minimum was 0.101 m, and the average mean square error was 0.121 m (121 mm).

c: ERROR SOURCES AND ANALYSIS

(1) Influencing factors of UAV photogrammetry accuracy

① UAV flight control technology: When performing aerial photography, UAV is highly affected by airflow, wind force, and wind direction. The UAV is unstable in flight, which affects the image quality and photogrammetry accuracy.

② Photographic camera quality:

Camera objective lens has significant chromatic aberration and distortion: The camera objective lens produces lateral and vertical chromatic aberrations in the focal plane because of the different refractive index of the light, resulting in the blurred and unclear images. Some residuals exist in the production, installation, and debugging of the camera objective. The distortion difference cannot retain the exact similarity between the image and the object, resulting in the geometric deformation of the image.

Chip size of CCD and Resolution: Resolution implies the analytical ability of a CCD chip of a digital camera to the object. The number of pixels is a crucial factor in measuring the resolution of a digital camera. In the same area, the more pixels are (namely the unit pixels are smaller), the higher resolution of the image is, the better detail performance of the image is, and the more realistic color restoration is. Else, the image quality is worse.

③ Measurement technical scheme

Image overlap, ratio of baseline and height: A majority of small digital cameras used by UAV are rectangular array CCD, not traditional square. The larger the image overlap is, the smaller the ratio of the baseline and height is. In the 3D model, the intersection angle of the same objects can be smaller, which decreases the 3D observation effect and directly affects the accuracy of the elevation measurement.

Image control point target selection: When image control points are measured, the richness of the image texture (such as rough image texture and curved surface features) directly affects the accuracy of the points selection. Moreover, indoor operation exerts a significant impact on puncturing image control points, which decreases the accuracy.

(2) The main methods to enhance the UAV photogrammetry accuracy are as follows:

① Enhance the accuracy of image control points: Improving the accuracy of image control points includes the measurement accuracy of image control points and the accuracy of image control point target selection such as using high-precision GPS to measure image control points; enhance the distribution density and uniformity of image control points.

② Improve the accuracy of camera distortion parameters: First, detect the camera distortion parameters before and after UAV aerial photogrammetry; second, fix the camera lens to decrease the impact caused by camera distortion parameter changes on the measurement results.

③ Improve image clarity: The UAV aerial image clarity is affected by flight speed, camera shutter speed, and flight turbulence. UAV fly at uniform speed as much as possible (the speed is controlled within 80 km/h), adjust the appropriate camera shutter speed, camera exposure time, and ISO value of the camera to decrease image noise.

④ Choose the appropriate flight altitude: The flight altitude primarily affects the GSD (ground sampling resolution) in the flight image, and the change of flight altitude inevitably affects the size of the aerial image. The closer the UAV is to the ground, the smaller the GSD value is, and the higher the accuracy is. The design of aerial height could be as follows:

$$H = \frac{f \times GSD}{\alpha} \tag{13}$$

TABLE 6. Mean square error of subsidence obtained by UAV.

	Subsidence accuracy of 1~2 UAV data			Subsidence accuracy of 1~3 UAV data			Subsidence accuracy of 2~3 UAV data		
	Subsidence of total station /m	Subsidence of UAV/m	Subsidence difference /m	Subsidence of total station /m	Subsidence of UAV/m	Subsidence difference /m	Subsidence of total station /m	Subsidence of UAV/m	Subsidence difference /m
1	0.138	0.057	-0.08	-0.131	-0.063	0.067	0.007	-0.005	-0.012
2	1.917	1.865	-0.051	-1.968	-1.936	0.031	-0.051	-0.071	-0.02
3	0.224	0.133	-0.09	-0.199	-0.455	-0.256	0.025	-0.321	-0.346
4	0.746	0.603	-0.142	-0.75	-0.532	0.217	-0.004	0.0701	0.0741
5	0.166	0.007	-0.158	-0.101	0.07	0.171	0.065	0.078	0.013
6	0.124	-0.025	-0.149	-0.06	0.137	0.197	0.064	0.112	0.048
7	0.181	0.061	-0.119	-0.11	0.013	0.123	0.071	0.074	0.003
8	0.077	0.129	0.052	-0.087	-0.047	0.039	-0.01	0.082	0.092
9	0.101	0.045	-0.055	-0.163	-0.016	0.146	-0.062	0.028	0.09
10	1.136	1.112	-0.023	-2.244	-2.087	0.156	-1.108	-0.975	0.132
11	1.699	1.679	-0.019	-2.264	-2.21	0.044	-0.565	-0.539	0.025
12	0.039	-0.079	-0.118	-0.068	-0.011	0.056	-0.029	-0.091	-0.062
13	0.098	-0.02	-0.12	-1.059	-1.105	-0.046	-0.961	-1.13	-0.169
	Mean square error/m：0.101m			Mean square error/m：0.140m			Mean square error/m：0.123		

TABLE 7. The PMS obtained by the data of September, 2018.

Subsidence factor/q	Tangent of major influence angle/tanβ	Propagation angle/θ (°)	Left deviation of inflection point/S1 (m)	Right deviation of inflection point/S2 (m)	Upper deviation of inflection point/S3 (m)	Lower deviation of inflection point/S4 (m)
0.76	2.7	88.9	16.6	27.7	14.4	-10.3

where H is the height of the photography row (m); f is the lens focal length (mm); a is the pixel size (mm); and GSD is ground sampling resolution (m).

D. SUBSIDENCE PARAMETERS INVERSION

In this study, we used the measured subsidence value of UAV to inverse the probability integral parameters. The SDSB [Figure 7(a)] can be obtained by subtracting DEM data of UAV in phases 2 (September 3, 2018) and 1 (June 9, 2018). Furthermore, we obtained the PMS by using the DPM established in Section III of this paper, Table 7 shows the measured PMS. As shown in Figure 8(a), making a profile along the centerline of the subsidence basin along the strike (A–A′)/dip (B–B′) main section, the tangents were extracted and compared with the predicted values. During June 9−September 3, 2018, when the coal seam was excavated to 640 m, the maximum measured subsidence value was 2135 mm, and the predicted subsidence value was 2198 mm. Based on the comparison between the measured and predicted results, the mean square error of the subsidence in the entire area was 124 mm, accounting for 5.8% of the maximum subsidence value [Figure 8(a)]. As shown in Figure 8(b)and (c), the two sections fit well. The error of the strike profile fitting was 112 mm, accounting for 5.2% of the maximum strike subsidence value. The error of the dip profile fitting was 136 mm, accounting for 6.3% of the maximum dip subsidence value.

E. SIMULATION ANALYSIS OF PMS RELIABILITY

As mentioned earlier, the average mean square error of the subsidence value obtained by UAV was 121 mm, and the maximum mean square error was 142 mm. The monitoring precision of a single point did not meet the requirements of the relevant specification. Simulation analysis was used to study the reliability of PMS. By adding random error to the subsidence value, the PMS is calculated by using the subsidence value after adding error, we analyzed the effect of measurement error on the PMS, and then received the reliability of PMS.

Taking the observation station of a working face as an example, we illustrated the impact of the observation error on PMS. Figure 9(a) shows the layout of the observation station; for this observation station, traditional leveling method was adopted for observation, the measured subsidence value of the observation station is presented in Table 8. The PMS is presented in the first row of Table 9, and Figure 9(b) and (c) show subsidence fitting.

The measured subsidence value of the observation station was considered as the true value, and the calculated parameters were regarded as the true value of the parameters. Then, the random error was added to the subsidence value, and the parameters were calculated by the subsidence value after adding error. Through comparative analysis, the impact of errors on the PMS of mining was obtained, as shown in Table 9.

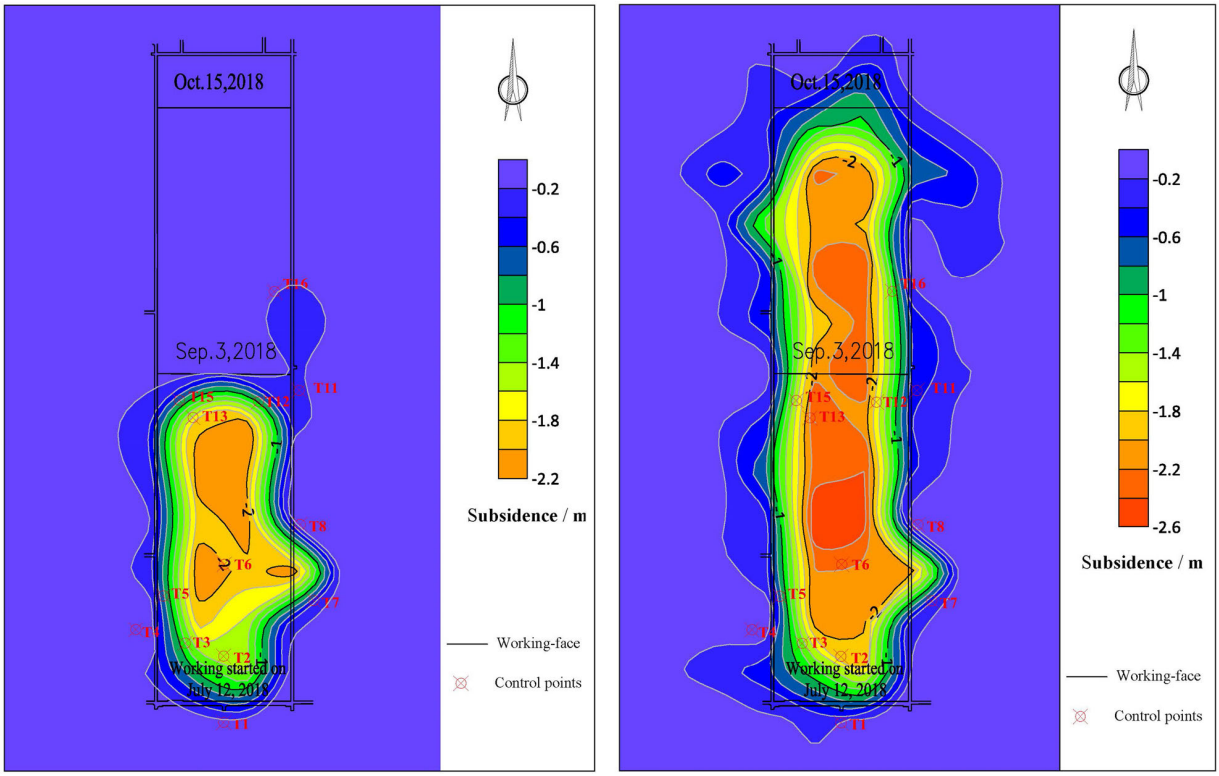

FIGURE 7. The SDSB from phase I (2018.06.09) to phase II (2018.09.03) and the SDSB from phase I to phase III (2018.10.15).

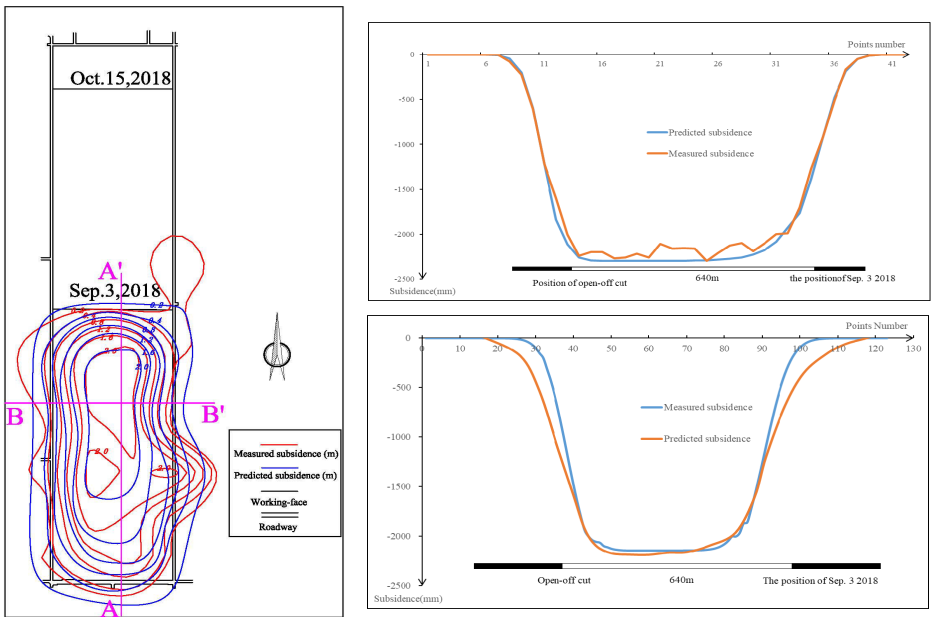

FIGURE 8. The comparison between predicted subsidence and measured dynamic subsidence during June 9-September 3, 2018. (a) The comparison of the whole subsidence basin; (b)the profile of the strike direction main section (A-A′); (c) the profile of the dip direction main section (B–B′).

As revealed in Table 9, when the mean square error is within the range of (1%–10%)W_0(W_0 is the maximum measured subsidence value), namely 10–60 mm, the subsidence coefficient remained stable. When out of range, the subsidence coefficient deviated from the true value. When the mean square error was within the range of (1%–7%) W_0, namely 10–40 mm, the calculated parameters were reliable. When the mean square error was >7%, the deviation of

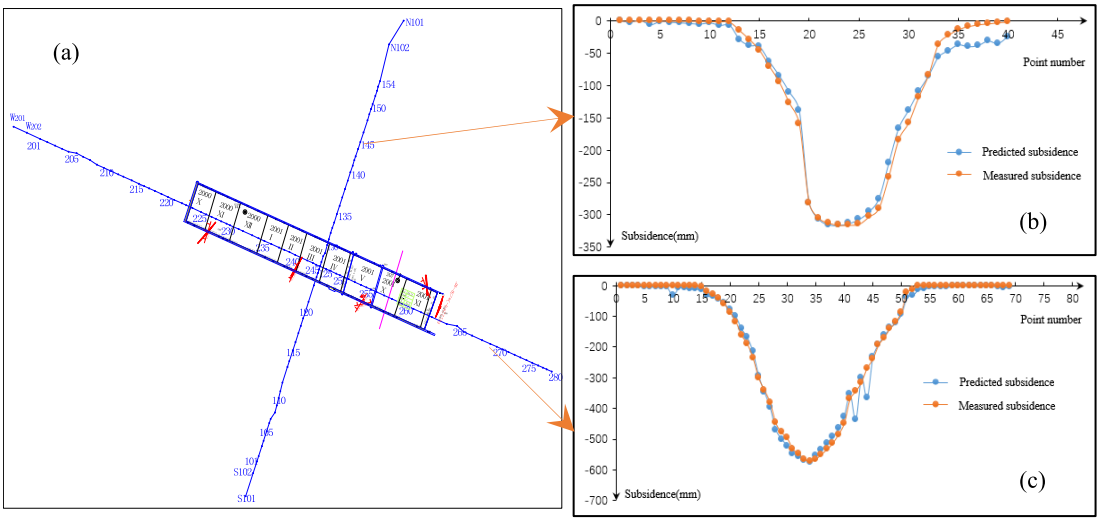

FIGURE 9. The surface subsidence observation station and the subsidence fitting; (a) the top and bottom view of the observation station; (b) Subsidence fitting in the strike direction (c) subsidence fitting in the dip direction.

TABLE 8. Field subsidence value of the observation station.

The observation line along the strike direction								The observation line along the dip direction			
Points	subsidence	**Points**	subsidence	**Points**	subsidence	**Points**	subsidence	**Points**	subsidence	**Points**	subsidence
No.	/mm	No.	/mm	No.	/mm	No.	/mm	No.	/mm	No.	/mm
1	0	17	36	33	568	49	121	1	3	17	295
2	0	18	43	34	575	50	93	2	7	18	275
3	0	19	58	35	555	51	37	3	7	19	220
4	2	20	78	36	536	52	31	4	29	20	166
5	3	21	100	37	513	53	13	5	38	21	138
6	3	22	140	38	493	54	9	6	40	22	109
7	3	23	168	39	465	55	4	7	63	23	85
8	4	24	215	40	426	56	3	8	85	24	56
9	5	25	293	41	354	57	3	9	110	25	46
10	32	26	346	42	438	58	4	10	139	26	37
11	7	27	397	43	301	59	1	11	281	27	40
12	7	28	470	44	367	60	0	12	307	28	38
13	10	29	500	45	233	61	0	13	315	29	31
14	11	30	523	46	191	62	0	14	316	30	35
15	12	31	547	47	163			15	313	31	24
16	31	32	558	48	138			16	307		

inflection point deviated markedly from the true value (when the mean square error was 40, $SI = 41$, deviated 11 m from the true value). Table 9 also shows that the effect of the mean square error on the tangent of the main influence angle and the mining transference angle was not significant. When the mean square error was within the range of (1%–10%), fitting mean square error fulfilled the requirement of $<0.1W_0$. If the mean square error was out of this range (1%–10%), fitting mean square error was larger than $0.1W_0$(in the table, when mean square error is 70 mm, the fitting mean square error is 72 mm, which is larger than $0.1W_0 = 57.5$ mm; at this time, the calculated parameters are not reliable).

As analyzed above, when the ratio of the mean square error to the maximum measured subsidence value was <7%, all of the PMS were reliable. When the ratio of the observation mean square error to the maximum measured subsidence value was 7%–10%, the calculated subsidence coefficient, the tangent of the main influence angle, and the mining transference angle were reliable. Conversely, the deviation of the inflection point deviated markedly from the true value. When the ratio of the error to the maximum subsidence value was >10%, all of the PMS was not reliable.

Based on the analysis explained above, Table 10 shows the effect of observation errors on the reliability of the calculated parameters using the PIM. Thus, when the ratio of the mean square error to the maximum subsidence value was <7%, all the parameters obtained were reliable. When the ratio of the mean square error to the maximum subsidence value was 7%–10%, some parameters obtained were reliable, while those >10% were unreliable.

From the perspective of parameters acquisition, the surface subsidence observed by UAV in Wangjiata coal mine could be

TABLE 9. The PMS after adding random error.

Observation mean square error/mm	Subsidence factor q	Tangent of major influence angle $tan\beta$	Propagation angle θ (°)	Left deviation of inflection point $S1$ (m)	Right deviation of inflection point $S2$ (m)	Upper deviation of inflection point $S3$ (m)	Lower deviation of inflection point $S4$（m）	Mean square error of fitting /mm
True value of PMS	0.52	1.84	89.17°	29.41	110.19	18.53	17.58	18.2
10	0.51	1.87	88	21.02	104.37	19.22	20.35	22
20	0.52	1.87	88	27.55	111.05	20.68	17.43	28
30	0.51	1.91	88	33.62	110.11	20.6	18.44	33
40	0.52	1.87	88	41.09	110.11	16.98	17.66	41
50	0.50	1.84	88	44.31	118.85	15.69	18.80	54
60	0.50	1.82	88	10.88	103.13	20.22	16.81	56
70	0.48	1.84	88	18.62	103.08	18.29	18.77	72
80	0.52	1.84	89	48.33	113.74	11.30	17.97	120
90	0.54	1.99	89.7	0.21	116.30	16.30	18.53	192

Note: the mean square error $m = \sqrt{[vv]/(n-1)}$, $v = W_1 - W_2$, where W_1 is the subsidence value after adding error and W_2 is the measured parameters through calculation.

TABLE 10. The effect of measurement errors on the reliability of the PMS.

The ratio of the mean square error to the maximum measured subsidence value	Subsidence factor/q	Tangent of major influence angle/$tan\beta$	Propagation angle /θ（°）	deviation of inflection point/S（m）
<7%	Reliable	Reliable	Reliable	Reliable
7%~10%	Reliable	Reliable	Reliable	Unreliable
>10%	Unreliable	Unreliable	Unreliable	Unreliable

used to monitoring subsidence deformation if the following conditions were fulfilled:

$$\frac{121mm}{W_0} = 7\% \Rightarrow W_0 = 1729mm$$
$$\frac{121mm}{W_0} = 10\% \Rightarrow W_0 = 1210mm$$

Specifically, the application of UAV in mining subsidence monitoring needs to fulfill one requirement. The maximum surface subsidence in the observation area was >1729 mm; if the maximum subsidence was 1210–1729 mm, some parameters were reliable.

Based on the comparison between the measured and predicted results in Sections of IV-C and D of this paper, the observed maximum subsidence value of Wangjiata coal mine was 2135 mm by September 3, 2018 and 2670 mm by October 15, 2018, the mean square error of the subsidence in the entire area was 124 mm, accounting for 5.8% of the maximum subsidence value by September 3, 2018, the ratio of the mean square error to the maximum subsidence value was <7%, based on the analysis presented above, it can be concluded that the PMS obtained by inversion of the measured subsidence value by UAV Photogrammetry technology in the Wangjiata coal mine are reliable. In addition, UAV monitoring was used to obtain the subsidence value of the entire area. Although the monitoring precision of a single point was not high, the PMS could be obtained by using a large number of entire subsidence basin data in the area that has better resistance to errors, and the calculated parameters can also obtain high precision.

Thus, we used 3 months (2018.06.09 -2018.09.03), the working face 2S201 of the Wangjiata coal mine were selected to monitor two to three times, DEM of each period was attained through data processing. Then, the information data on the entire basin of the dynamic subsidence area was obtained by DEM subtraction of two periods. The reliable PMS were obtained quickly. Therefore, UAV Photogrammetry technology can not only enhance the efficiency but also obtain comprehensive measured data of subsidence basin. Besides, this method provides precise predicted parameters for mining subsidence. Hence, UAV Photogrammetry technology offers a broader application prospect in the mining area because it can better predict surface subsidence.

V. CONCLUSIONS

The research findings of this study are as follows:

(1) As a new monitoring technology for mining subsidence, UAV Photogrammetry technology overcomes the

limitations, including a long observation period, high labor intensity, burying fixed measuring points, and difficult protection in traditional observation stations. UAV Photogrammetry technology can be used to obtain ground dynamic subsidence basin data in mining area in a short time. In addition, the ground subsidence parameters are calculated reliably by the probability integral dynamic prediction model and dynamic parameters acquisition method. Besides improving the efficiency, UAV Photogrammetry technology offers rich subsidence data, which provides crucial data support for environmental assessment, land reclamation, and ecological restoration in the mining area.

(2) The research results suggest that the average mean square error of DEM obtained by UAV is 118 mm, and the average mean square error of the subsidence value is 121 mm. UAV photogrammetry technology monitoring is used to obtain the subsidence value of the entire area. Although the monitoring precision of a single point is not high, the PMS can be obtained by using a large number of the entire subsidence basin data which has a better resistance to errors, and the calculated parameters can also obtain high precision.

(3) Through systematic studies, a set of complete technical system for monitoring surface subsidence in the mining area by UAV Photogrammetry technology and quickly obtaining the parameters of mining subsidence is formed. As the method has been successfully applied in Wangjiata coal mine of Inner Mongolia of China, it merits promotion and application.

AUTHOR CONTRIBUTIONS

Zhou Dawei proposed the basic idea of dynamic subsidence monitoring and wrote the paper. Qi Lizhuang and Zhang Demin designed the mining subsidence observation station and revised the paper. Guo LiangLin and Zhou Baohui analyzed the data of UAV image and performed the UAV field surveying.

ACKNOWLEDGMENT

The authors would like to thank Z. Zhaojiang from Hebei University of Engineering providing the help in field data acquisition of UAV Images. The authors are also grateful to the reviewers of this paper for their comments.

REFERENCES

[1] G. He, L. Yang, G. Ling, C. Jia, and D. Hong, *Mining Subsidence Science*. Xuzhou, China: China Univ. Mining and Technology Press, 1991.

[2] H. Kratzsch, *Mining Subsidence Engineering*. New York, NY, USA: Springer-Verlag, 1983.

[3] K. Wu, J. X. Ge, L. D. Wang, and M. Zhou, *Unify Method of Mining Subsidence Prediction*. Xuzhou, China: China Univ. Mining and Technology Press, 1998.

[4] B. H. G. Brady and E. T. Brown, *ROCK Mechanics for Underground Mining*, 3rd ed. London, U.K.: Springer, 2004.

[5] D. Zhou, K. Wu, X. Miao, and L. Li, "Combined prediction model for mining subsidence in coal mining areas covered with thick alluvial soil layer," *Bull. Eng. Geol. Environ.*, vol. 77, no. 1, pp. 283–304, Feb. 2018.

[6] L. Yuan, K. Wu, G. Du, and Z. Tan, "Monitoring of Huaihe Dike deformation caused by mining," *J. China Univ. Mining Technol.*, vol. 11, no. 1, pp. 14–19, 2001.

[7] D. Zhou, K. Wu, L. Li, X. Diao, and X. Kong, "A new methodology for studying the spreading process of mining subsidence in rock mass and alluvial soil: An example from the Huainan coal mine, China," *Bull Eng Geol Environ*, vol. 75, no. 3, pp. 1067–1087, Aug. 2016, doi: 10.1007/s10064-016-0877-3.

[8] D. Zhou, K. Wu, R. Chen, and L. Li, "GPS/terrestrial 3D laser scanner combined monitoring technology for coal mining subsidence: A case study of a coal mining area in Hebei, China," *Natural Hazards*, vol. 70, no. 2, pp. 1197–1208, Jan. 2014, doi: 10.1007/s11069-013-0868-7.

[9] S. S. Peng, *Surface Subsidence Engineering*. New York, NY, USA: Littleton Society for Mining, Metallurgy, 1992.

[10] K. Wu, Y. Wang, and S. Wang, *New Technology for Mine Subsidence Monitoring and Prediction*. Beijing, China: China Environmental Science Press, 2012.

[11] X. Diao, K. Wu, D. Hu, L. Li, and D. Zhou, "Combining differential SAR interferometry and the probability integral method for three-dimensional deformation monitoring of mining areas," *Int. J. Remote Sens.*, vol. 37, no. 21, pp. 5196–5212, Nov. 2016, doi: 10.1080/01431161.2016.1230284.

[12] X. Diao, K. Wu, D. Zhou, and L. Li, "Integrating the probability integral method for subsidence prediction and differential synthetic aperture radar interferometry for monitoring mining subsidence in Fengfeng, China," *J. Appl. Remote Sens*, vol. 10, no. 1, Mar. 2016, Art. no. 016028, doi: 10.1117/1.jrs.10.016028.

[13] Y. Du, G. Feng, X. Peng, and Z. Li, "Subsidence Evolution of the Leizhou Peninsula, China, Based on InSAR Observation from 1992 to 2010," *Appl. Sci.*, vol. 7, no. 5, p. 466, May 2017, doi: 10.3390/app7050466.

[14] H. D. Fan, D. Cheng, K. Z. Deng, B. Q. Chen, and C. G. Zhu, "Subsidence monitoring using D-InSAR and probability integral prediction modelling in deep mining areas," *Survey Rev.*, vol. 47, no. 345, pp. 438–445, Nov. 2015, doi: 10.1179/1752270614y.0000000153.

[15] H. Fan, X. Gao, J. Yang, K. Deng, and Y. Yu, "Monitoring mining subsidence using a combination of phase-stacking and offset-tracking methods," *Remote Sens.*, vol. 7, no. 7, pp. 9166–9183, Jul. 2015, doi: 10.3390/rs70709166.

[16] C. Huang, H. Xia, and J. Hu, "Surface deformation monitoring in coal mine area based on PSI," *IEEE Access*, vol. 7, pp. 29672–29678, 2019, doi: 10.1109/access.2019.2900258.

[17] Z. F. Yang, Z. W. Li, J. J. Zhu, J. Hu, Y. J. Wang, and G. L. Chen, "InSAR-based model parameter estimation of probability integral method and its application for predicting mining-induced horizontal and vertical displacements," *IEEE Trans. Geosci. Remote Sens.*, vol. 54, no. 8, pp. 4818–4832, Aug. 2016, doi: 10.1109/tgrs.2016.2551779.

[18] Z. Yang, Z. Li, J. Zhu, H. Yi, J. Hu, and G. Feng, "Deriving dynamic subsidence of coal mining areas using InSAR and logistic model," *Remote Sens.*, vol. 9, no. 2, p. 125, Feb. 2017, doi: 10.3390/rs9020125.

[19] J. Zhu, Z. Li, and J. Hu, "Research progress and methods of InSAR for deformation monitoring," *Acta Geodaetica et Cartograph. Sinica*, vol. 46, no. 10, pp. 1717–1733, 2017.

[20] J. zhu, Z. Yang, and Z. Li, "Recent progress in retrieving and predicting mining-induced 3D displace-ments using InSAR," *Acta Geodaetica et Cartograph. Sinica*, vol. 48, no. 2, pp. 135–144, 2019.

[21] R. M. Mateos, J. M. Azañón, F. J. Roldán, D. Notti, V. Pérez-Peña, J. P. Galve, J. L. Pérez-García, C. M. Colomo, J. M. Gómez-López, O. Montserrat, N. Devantèry, F. Lamas-Fernández, and F. Fernández-Chacón, "The combined use of PSInSAR and UAV photogrammetry techniques for the analysis of the kinematics of a coastal landslide affecting an urban area (SE Spain)," *Landslides*, vol. 14, no. 2, pp. 743–754, Apr. 2017, doi: 10.1007/s10346-016-0723-5.

[22] H. Yao, R. Qin, and X. Chen, "Unmanned aerial vehicle for remote sensing applications-a review," *Remote Sens.*, vol. 11, no. 12, 2019, doi: 10.3390/rs11121443.

[23] A. Rauhala, A. Tuomela, C. Davids, and P. Rossi, "UAV remote sensing surveillance of a mine tailings impoundment in sub-arctic conditions," *Remote Sens.*, vol. 9, no. 12, p. 1318, Dec. 2017, doi: 10.3390/rs9121318.

[24] X. Tong, X. Liu, P. Chen, S. Liu, K. Luan, L. Li, S. Liu, X. Liu, H. Xie, Y. Jin, and Z. Hong, "Integration of UAV-based photogrammetry and terrestrial laser scanning for the three-dimensional mapping and monitoring of open-pit mine areas," *Remote Sens.*, vol. 7, no. 6, pp. 6635–6662, May 2015, doi: 10.3390/rs70606635.

[25] S. Li, L. Li, Z. Li, X. Chen, T. Fernando, H. H.-C. Iu, G. He, Q. Wang, and X. Liu, "Event-trigger heterogeneous nonlinear filter for wide-area measurement systems in power grid," *IEEE Trans. Smart Grid*, vol. 10, no. 3, pp. 2752–2764, May 2019, doi: 10.1109/tsg.2018.2810224.

[26] B. Liu, Z. Li, X. Chen, Y. Huang, and X. Liu, "Recognition and vulnerability analysis of key nodes in power grid based on complex network centrality," *IEEE Trans. Circuits Syst. II, Exp. Briefs*, vol. 65, no. 3, pp. 346–350, Mar. 2018, doi: 10.1109/tcsii.2017.2705482.

ZHOU DAWEI was born in Henan, China, in 1984. He received the M.Eng. degree in mining subsidence and subsidence control engineering and the Ph.D. degree in geodesy and surveying engineering from the China University of Mining and Technology, Xuzhou, China, in 2011 and 2014, respectively.

From 2015 to 2017, he was a Postdoctoral Fellow with the China University of Mining and Technology. He joined RWTH Aachen University, Germany, as a Visiting Research Scholar, in 2016. He is currently a Full Associate Professor with the China University of Mining and Technology. His research interests include mining subsidence and its control, rock mass movement and control, the application of 3D laser scanner, UAV, and InSAR Technology in deformation monitoring of coal mining area.

QI LIZHUANG received the B.S. degree in surveying and mapping engineering from the China University of Mining and Technology, Xuzhou, China, in 2017, where he is currently pursuing the M.S. degree in geodesy and surveying engineering.

His current research interests include the application of 3D laser scanner, UAV, and InSAR Technology in deformation monitoring of mining area.

ZHANG DEMIN was born in Hebei, China, in 1961. He received the degree in mine surveying from the Beijing Coal Mine School (now known as Beijing Polytechnic College), Beijing, China, in 1983, and the B.S. degree in engineering surveying from Wuhan University, Wuhan, in 1991.

From 1983 to 2008, he was a Surveying Technician, an Engineer, and the Survey Chief with the Linxi Mine and Qianjiaying Mine of Hebei Kailuan Group, respectively. Since 2008, he has been the Surveying Engineer of the Xin'ao Group, Xinneng Mining Industry Co., Ltd. His research interests include mining subsidence, rock mass movement and control, and underground connection surveys.

ZHOU BAOHUI was born in Inner Mongolia, China, in 1990. He received the B.S. degree in surveying and mapping engineering from the Inner Mongolia University of Science and Technology (MUST), Baotou, China, in 2014, where he is currently pursuing the M.S. degree in geodesy and surveying engineering.

From 2014 to 2018, he was a Surveying Technician with Xinneng Mining Industry Co., Ltd. (XMIC), Ordos City, China. He is currently a Survey Engineer with XMIC. His research interests include engineering survey, mining subsidence, the application of 3D laser scanner, UAV, and InSAR Technology in deformation monitoring of coal mining area.

GUO LIANGLIN received the B.S. degree in surveying engineering from the Anhui University of Science and Technology, in 2018. He is currently pursuing the M.A. degree in surveying engineering with the China University of Mining and Technology, Xuzhou, China.

His current research interests include the principles and applications of 3D laser scanning technology, mining subsidence, and tunnel support.